Preprint
UCRL-JC-151135

Assessment of Proton Microbeam Analysis of ^{11}B for Quantitative Microdistribution Analysis of Boronated Neutron Capture Agent Analogs in Biological Tissues

G. Bench, P. G. Grant, D. L. Ueda, S. A. Autry-Conwell, Y. Hou, J. E. Boggan

U.S. Department of Energy

Lawrence Livermore National Laboratory

This article was submitted to
American Geophysical Union Fall 2002, San Francisco, CA,
December 6-10, 2002

December 4, 2002

This work was performed under the auspices of the United States Department of Energy by the University of California, Lawrence Livermore National Laboratory under contract No. W-7405-Eng-48.

Assessment of proton microbeam analysis of ^{11}B for quantitative microdistribution analysis of boronated neutron capture agent analogs in biological tissues

Graham Bench[1]* (Ph.D.), Patrick G. Grant[1] (Ph.D.), Dawn L. Ueda[1] (B.S.), Susan A. Autry-Conwell[2] (MBA), Yongjin Hou[3] (M.D.) and James E. Boggan[3] (M.D.)

[1] Center for Accelerator Mass Spectrometry, Lawrence Livermore National Laboratory, Livermore CA 94551, U.S.A.

[2] Center for Biophotonics Science & Technology, University of California, Davis, Sacramento CA 95817, U.S.A.

[3] Department of Neurological Surgery, University of California, Davis, Sacramento CA 95817, U.S.A.

*Corresponding Author: Graham Bench

Center for Accelerator Mass Spectrometry, L-397

Lawrence Livermore National Laboratory,

Livermore, CA 94551

Phone: (925)-423-5155

Fax: (925)-423-7884

Email: bench1@llnl.gov

Acknowledgements: This work was partially performed under the auspices of the U.S. Department of Energy by Lawrence Livermore National Laboratory under contract W-7405-ENG-48, DOE grant 98ER62576 Center of Excellence for Laser Applications in Medicine, and from a CAMS minigrant.

Running Title: Proton microbeam analysis of ^{11}B in biological tissues

Abstract

Purpose: To assess the $^{11}B(p, \alpha)^{8}Be^{*}$ nuclear reaction for quantitatively mapping the *in-vivo* sub-cellular distribution of boron within gliosarcoma tumors treated with boronated neutron capture therapy agent (NCTA) analogs.

Materials and Methods: Intracranial tumors were produced in Fisher 344 rats using a 9L gliosarcoma model. Fourteen days later, the majority of rats were treated with f-boronophenylalanine and sacrificed 30 or 180 minutes after intravenous injection. Freeze dried tumor cryosections were imaged using the $^{11}B(p, \alpha)^{8}Be^{*}$ nuclear reaction and proton microbeams obtained from the nuclear microprobe at Lawrence Livermore National Laboratory.

Results/Discussion: With $^{11}B(p, \alpha)^{8}Be^{*}$ analysis, ^{11}B distributions within cells can be quantitatively imaged with spatial resolutions down to 1.5 μm, minimum detection limits of 0.8 mg/kg and acquisition times of several hours. These capabilities offer advantages over alpha track autoradiography, electron energy loss spectroscopy and secondary ion mass spectrometry (SIMS) for ^{11}B quantitation in tissues. However, the spatial resolution, multi-isotope capability and analysis times achieved with SIMS are superior to those achieved with $^{11}B(p, \alpha)\ ^{8}Be^{*}$ analysis.

Conclusions: When accuracy in quantitation is crucial, the $^{11}B(p, \alpha)\ ^{8}Be^{*}$ reaction is well suited for assessing the microdistribution of ^{11}B. Otherwise, SIMS may well be better suited to image the microdistribution of boron associated with NCTAs in biological tissues.

Key words/phrases: BNCT, boron, proton microbeam analysis, quantitative microdistribution.

Introduction

Greater than 10,000 cancer deaths per year in the United States can be attributed to primary brain tumors [1,2]. In children, brain tumors are the most common type of solid tumor, and are second only to leukemia in overall incidence of malignancy [3,4]. Despite advances in surgery, radiotherapy and chemotherapy, median survival time for adults with glioblastoma multiforme or aggressive anaplastic astrocytomas continues to be less than one year in most clinical reports [5]. The poor outcome in response to multi-modality treatment of malignant brain tumors indicates the need for further research in areas that may hold promise for affected patients [6]. The majority of brain tumor recurrences are located within 2 cm of the original tumor boundary, which suggests that an improvement in outcome might be expected if a more efficacious local therapy were available [7].

Neutron capture therapy (NCT) is a binary therapeutic modality that has potential for treatment of localized tumors [8,9,10]. NCT relies on selective uptake and or retention within a tumor of a neutron capture agent (NCA). NCAs are non-toxic drugs containing a neutron capture element (NCE) such as ^{10}B or gadolinium. During irradiation with a neutron beam, thermal neutrons are absorbed (captured) by ^{10}B creating an unstable ^{11}B compound nucleus that immediately breaks up to yield a recoiling alpha particle (1.47 MeV) and ^{7}Li nuclei (0.84 MeV):

$$^{10}B + n_{th} \longrightarrow [^{11}B] \longrightarrow {}^{4}He + {}^{7}Li\ (2.31\ MeV).$$

In 94% of boron neutron captures, a 480 keV prompt gamma ray is emitted in addition to the ^{4}He and ^{7}Li particles. Because the ^{4}He and ^{7}Li particles produced are high linear energy transfer (high-LET) particles, damage is largely confined to a radius of 4 to 14 μm and thus localized to cells in which the neutron capture reactions occur. Cell damage caused by high-LET particles is not repaired or affected by hypoxia [8] and one capture event may liberate enough energy to kill a cell. NCT could be efficacious in the treatment of brain and other localized tumors if the high-LET radiation dose is confined to malignant cells and the total radiation dose to normal tissues kept below a threshold for significant radiation injury [11,12]. However, a number of issues require resolution before NCT can be accepted as a primary modality in the management of malignant brain tumors and other localized neoplasms [13].

One key to the success and acceptance of NCT as a primary treatment modality is the development of new non-toxic NCA compounds with localization in or near vital tumor cell structures. Ideally, a NCA should reach a uniform distribution and high concentration within all tumor cell nuclei or vital organelles regardless of tumor cell location. A NCA should also be retained by the tumor for a therapeutically advantageous period, be excluded from normal tissues and cleared from the blood and vascular endothelium prior to irradiation. For instance, prolongation of survival and tumor cures have been reported using boronated phenylalanine (BPA) NCT in rodent tumor models [14,15,16,17,18]. Administration of 1500 mg/kg BPA in a rat 9L gliosarcoma brain tumor model resulted in 39, 12, and 10 μg of ^{10}B/g in tumor, blood, and brain at the time of treatment with thermal neutrons [19]. Fifty percent of the treated rats were cured of tumors with minimal evidence of brain injury one year after treatment.

The short range of ionizing particles produced in NCT makes localization of the NCA important for efficacy. The increasing recognition of subcellular boron distribution as an important parameter in agent evaluation has led to studies of the suitability of several analytical procedures for mapping boron microdistribution in biomedical tissues. These procedures have included α-track autoradiography [20], electron energy loss spectroscopy [21] and secondary ion mass spectrometry [22].

It is also possible to detect boron via nuclear reaction analysis using incident MeV energy protons. For the analysis of ^{10}B, photon-tagged nuclear reaction analysis (pNRA) can be employed [23]. This method is based on the detection of scattered particles in coincidence with a de-excitation gamma photon. However, the pNRA cross-section of $\leq$ 1 mbarn from ^{10}B is not sufficient for a time efficient analysis of the microdistribution of boron in biomedical tissues [23]. In addition, the reaction produces typical minimum detection limits of > 10 mg/kg ^{10}B in biological tissues.

Although ^{10}B is the neutron capture element for boron containing NCAs ^{10}B and ^{11}B are thought to be similar in a chemical and biological sense [24]. Organ and cellular uptake and distribution of ^{10}B labeled NCAs has been shown to be similar to that of the corresponding ^{11}B labeled analogs [22]. This implies that it should be possible to study the subcellular localization of boron containing NCAs by quantitating ^{11}B levels in biomedical tissues dosed with boronated NCA analogs.

^{11}B can be detected in biomedical tissues with the $^{11}B(p, \alpha)^{8}Be^{*}$ nuclear reaction [23]. This reaction has a cross-section of ~ 300 mbarn [23] at incident proton energies of 500 to 700 keV. This reaction has been used to measure boron in materials science specimens [25] and bulk boron contents of biological tissues [26]. The reaction has also been investigated for its suitability in quantitatively measuring levels of ^{11}B associated with boronated NCA analogs in biological tissues [23] and has a ^{11}B minimum detection limit of ~ 0.5 mg/kg. The relatively large cross-section implies tractable analysis times for microdistribution measurements of ^{11}B associated with boronated NCA analogs in biological tissues. This suggests that further investigation of the $^{11}B(p, \alpha)^{8}Be^{*}$ to quantitatively measure the micron scale distribution of ^{11}B within tumor cells treated with boronated NCA analogs is warranted.

In this study we explore the $^{11}B(p, \alpha)^{8}Be^{*}$ reaction to quantitatively map the micron scale distribution of boron within cells from rodent tumors treated with boronated NCA analogs. The methodology developed for such measurements is presented. Minimum detection limits, spatial resolution and analysis times for detection of ^{11}B in tumor tissues are discussed. Images showing the quantitative subcellular distribution of boronated NCA analogs in a rodent tumor model are presented. Finally, a comparison between the $^{11}B(p, \alpha)^{8}Be^{*}$ imaging technique and other techniques that have been investigated for their suitability in mapping the microdistribution of boron in tumor tissues is made.

Methods and materials

^{11}B microanalysis.

Incident protons are used to measure ^{11}B within a sample using the $^{11}B(p, \alpha)\ ^{8}Be^*$ nuclear reaction : $H + {}^{11}B \rightarrow \alpha_1 + {}^{8}Be^*$ and ${}^{8}Be^* \rightarrow \alpha_{11} + \alpha_{12}$. This nuclear reaction has a broad resonance at an incident proton energy of 630 keV. The reaction creates a compound nucleus, which decays into an excited state of ^{8}Be ($^{8}Be^*$) and an alpha particle. $^{8}Be^*$ can subsequently decay into two alpha particles. The emitted alpha particles have an energy distribution ranging from 0 to 6 MeV.

The nuclear microprobe at Lawrence Livermore National Laboratory (LLNL) [27] was used to produce incident proton beams ranging in energy from 450 to 750 keV to investigate this reaction. Alpha particle detection was accomplished with two 450 mm^2 silicon surface barrier particle detectors. Each detector was located 25 mm from the sample and subtended a mean scattering angle of 135^0. The total solid angle subtended by the two detectors was 1.6 Sr. Particles were recorded in list mode along with coincident beam spatial co-ordinates arising from electrostatically scanning the beam. Charge was collected in a Faraday cup located behind the sample. Figure 1 shows a schematic diagram of the experimental arrangement. Data were reduced off-line and spectra from features of interest within scanned regions were extracted and analyzed using the IMAP analysis code [28].

^{11}B standards and tissue blanks.

An 1800 angstrom thick B_5N film containing 50 +/- 5 $\mu g/cm^2$ ^{11}B served as a thin film standard. This standard was examined using incident proton beam energies of 450, 500, 550, 600, 630, 650, 700 and 750 keV. For each proton energy, a 500 x 500 μm^2 area of the film was scanned with a beam spot diameter of 5 μm. Beam currents were < 1 nA and the integrated charge in each scan was up to 1 μC.

Liver tissue sections from a Fischer F344 rat were used as tissue blanks for proton analysis. A liver was excised from a rat euthanized with carbon dioxide, frozen in liquid nitrogen and stored at –80 ^{o}C. Half of the liver was analyzed by inductively coupled plasma mass spectrometry (ICPMS) (Hewlett

Packard 4500) as previously described [29]. ICPMS revealed the ^{11}B content of the liver to be < 0.1 mg/kg. As the $^{11}B(p, \alpha)\ ^{8}Be^*$ reaction has a sensitivity of ~1 mg/kg for ^{11}B [23] this data suggested the liver would serve as an effective tissue blank for the proton irradiations. Ten μm thick cryosections were cut from the remaining tissue, placed on Formvar films and freeze dried as previously described [30].

Preparation of tumor samples.

9L animal model brain tumor preparation.

Fisher-344 rats (300 grams male) were anesthetized with ketamine (80 mg/kg) and xylazine (10 mg/kg) administered intraperitoneally in the lower right quadrant. Animals were placed into a stereotaxic frame and the drill site marked at: +1.0 mm caudal, 3.0-mm lateral of bregma. A 1 mm diameter hole was drilled through the skull and a 3 μl suspension of 50,000 9L cells injected into the brain, 4mm below the dura, by Hamilton syringe. Animals were hosted in an air-conditioned room with a 12 hour day and night cycle for two weeks before boron compound injection and tissue collection.

f-BPA solution preparation.

L-P Boronophenylalanine (BPA) (80 atom % ^{11}B, 20 atom % ^{10}B) was purchased from New Concept Therapeutics, Inc (Cary, NC). f-BPA (the fructose complex of BPA) [31] was prepared by adding the compound with 10% molar excess of fructose to water. The pH was slowly adjusted to between 9.5-10 with 5M NaOH by stirring the suspension until all solids were dissolved. The solution was then stirred for another 3 minutes. The pH was then adjusted to 7.4 by addition of HCl and stirred for 10 minutes. The volume of this solution was adjusted with deionized water to yield a 0.43 M solution (90 mg BPA/ml). This solution was stored at 4°C, and used within 24 hours.

f-BPA administration and animal sacrifice.

Fisher-344 rats were anesthetized with ketamine (80 mg/kg) and xylazine (10 mg/kg) administered intraperitoneally and fixed on a surgery board. Boron dosed rats were intravenously administered 3 ml of

0.43 M (90 mg/ml) f-BPA at a rate of 16 mL/hour by infusion pump. Undosed rats served as a control. Half the boron dosed rats were sacrificed 30 minutes after dosing while the other half were sacrificed 180 minutes after dosing. All rats were euthanized by administration of an overdose of isoflurane and immediately dissected. Tumors were removed, weighed, placed in cryotubes, frozen in liquid nitrogen and stored in a –80 ^{o}C freezer until cyrostat sectioning or digestion for ICP-MS.

For each animal, frozen tumors were cut in half. Half of each tumor was analyzed by ICPMS for boron as previously described [29]. Portions of remaining tumor samples were cryosectioned. Ten μm thick cryosections were placed on thin Formvar films and freeze dried as previously described [30]. Multiple tissue sections were produced from each tumor for nuclear microprobe analysis.

Nuclear microprobe analysis of tissue sections.

All tissue sections were analyzed using the $^{11}B(p, \alpha)\ ^{8}Be^{*}$ nuclear reaction and scanning transmission ion microscopy (STIM). STIM data is often collected with a nuclear microprobe to normalize elemental data so that accurate elemental concentrations can be obtained [30]. With STIM the residual energy of ions after traversing the specimen is measured by a particle detector located behind the sample. Because of the simple physics involved in ion energy loss mechanisms residual ion energies can be readily converted into specimen projected densities [32,33]. Because STIM is a highly efficient technique, low beam currents are utilized which make it possible to achieve sub-micron spatial resolution. These characteristics enable STIM to provide a rapid, histological assessment of the specimen [34].

STIM was utilized to select individual cells in tissue sections for subsequent boron analysis. STIM measurements were performed with an incident proton beam of energy 1.5 MeV focussed to a 0.5 micron diameter spot. To enable accurate conversion of energy losses to areal densities [32], a higher beam energy was used than that for boron analysis to ensure that proton energy loss was primarily via interactions with specimen electrons. Beam currents were a few thousand ions per second. At each beam location, the median value of 99 residual ion energies was selected to represent the average residual energy of the ion beam [32]. Residual ion energies were converted to specimen projected densities ($\mu g/cm^2$)

assuming the composition of the biological material was $C_5H_9O_2N$ [32,33]. This assumed composition has been shown have an accuracy to within 95% for converting residual ion energies to projected densities for a variety of biological matrices [33].

Tissues were analyzed for boron with an incident proton energy of 700 keV. Boron yields were obtained with ≤ 1.5 nA proton beams focussed down to spot sizes as small as 1.5 μm. Irradiation times were up to six hours and doses of up to 20 μC were deposited to interrogated areas. Alpha particle yields were converted to ^{11}B yields using data obtained from the 1800Å B_5N standard to produce boron yield maps with units of ng/cm^2. The resulting ^{11}B yield maps (ng/cm^2) were divided pixel by pixel by the registered STIM areal densities ($\mu g/cm^2$) to obtain mass normalized ^{11}B content maps in units of mg/kg. Up to six non-contiguous cells from each animal tumor were examined with this procedure.

Statistical analysis.

Potential differences in ^{11}B contents of individual cells or tumors from different treatment groups were assessed by unpaired two-tailed students t-tests. A significance level of < 0.05 was considered meaningful.

Results

Sensitivity, yields and backgrounds obtained with the $^{11}B(p, \alpha)\ ^{8}Be^*$ reaction.

Figure 2A shows the particle spectrum obtained from the irradiation of a liver tissue section with a 700 keV proton beam. Channel numbers on the horizontal axis have a linear relationship with particle energy and channel 1000 corresponds to approximately 7 MeV. Below channel 200, scattered protons from boron, nitrogen and associated pile-up peaks are present. Above channel 200, the spectrum contains less than 20 counts. Figure 2B shows the energy spectrum from the irradiation of the B_5N film with a 700 keV proton beam. The counts between channels 200 and 840 are the superposition of the alpha particle transitions from the $^{11}B(p, \alpha)\ ^{8}Be^*$ nuclear reaction. To determine boron yields with minimal contribution from scattered protons and instrumental noise, the number of events between channels 460 to 870 in each spectrum was selected. All events in this energy window were considered to be alpha particles arising from the $^{11}B(p, \alpha)\ ^{8}Be^*$ reaction. With this protocol, the yield obtained for the $^{11}B(p, \alpha)\ ^{8}Be^*$ reaction at an incident proton energy of 700 keV is 21,000 counts/$\mu g/cm^2/\mu C$.

Although alpha particles are detected below channel 460 they were not used to calculate yields. Owing to the thickness of the tissue sections many low energy alpha particles produced by the $^{11}B(p, \alpha)\ ^{8}Be^*$ reaction would not be detected as they would lose energy and be absorbed within the sample. Channel 460 corresponds to an alpha particle energy of ~ 3.2 MeV. Alpha particles with energies above 3 MeV are sufficiently energetic that they will not be stopped, independent of their depth of production, in tissue sections examined in this study. Selecting alpha particle yields between channels 460 and 870 helps ensure accurate boron quantitation in the tissue sections.

Figure 3 shows the $^{11}B(p, \alpha)\ ^{8}Be^*$ yield versus incident proton energy for the B_5N film. The predicted resonance has a peak value at 630 keV of 26,000 counts/$\mu g/cm^2/\mu C$. STIM revealed that all tissue sections had areal densities ranging between 500 and 600 $\mu g/cm^2$. For an incident energy of 700 keV, such target thicknesses result in residual proton energies of between 520 and 470 keV. Owing to the broad nature of the resonance the production cross–section over the energy range 470 to 700 keV varies

between 18,000 and 26,000 counts/μg/cm^2/μC. Consequently, if an incident proton energy of 700 keV is utilized to interrogate the tissue samples, alpha particle production from the $^{11}B(p, \alpha)\ ^{8}Be^*$ reaction can be considered to be constant to within +/-20 % at 22,000 counts/μg/cm^2/μC for the range of proton energies encountered as the incident beam traverses the sample.

The minimum detection limit (MDL) of an element is frequently defined as MDL = 3 $\sqrt{}$ Nb where Nb is the number of pulses in the background of the relevant signal. With this formalism, and assuming the alpha particle production cross-section from the $^{11}B(p, \alpha)\ ^{8}Be^*$ reaction is 22,000 counts/μg/cm^2/μC the yield from the liver tissue section in Figure 2A between channels 460 and 870 produces an MDL of 450 pg/cm2. STIM measurements with a 1.5 MeV proton beam revealed the tissue section to have a thickness of 550 μg/cm^2. Dividing the boron yield MDL by the tissue thickness yields a ^{11}B MDL of 0.8 mg/kg. Likewise, analysis of other liver tissue sections yielded ^{11}B MDLs of ~ 0.8 mg/kg.

Imaging of ^{11}B in tumor cells.

Figures 4, 5, and 6 show typical images obtained from proton microbeam analysis of tumor cells. In each image the color scale ranges from black (low), through gray (middle) to white (high). The range that the color scale spans in each image differs. The images in Figure 4 show the analysis of a tumor cell from a control rat not dosed with boron. The cell nucleus is visible towards the center of the scan. The average areal density in the scanned region was 570 +/- 30 μg/cm^2. The 700 keV proton irradiation produced an alpha particle yield of 265 events, which show as a random distribution in Figures 4C and 4D. This yield corresponds to an equivalent ^{11}B concentration of 0.7 mg/kg.

Figure 5 shows images of a tumor cell from a rat dosed with boron and sacrificed 30 minutes post dosing. The cell appears to have an oblong shape with major axis length of ~15 μm and minor axis length of ~10 μm. The cell nucleus is visible towards the center of the scanned region. The average areal density in the scanned region was 600 +/- 30 μg/cm^2. The 700 keV proton irradiation produced an alpha particle yield of 15983 counts. The ^{11}B yield map (Figure 5C) reveals a slightly elevated ^{11}B yield

(ng/cm^2) in the region corresponding to the location of the cell nucleus towards the center of the scanned region. However, once the ^{11}B yield map in normalized against mass, the resulting ^{11}B concentration map (Figure 5D) shows a homogeneous distribution throughout the cell. The average ^{11}B concentration in the cell is 58 +/- 14 mg/kg. ^{11}B concentrations were distributed homogeneously throughout all tumor cells analyzed from animals sacrificed 30 minutes post dosing.

Figure 6 shows images of a tumor cell from a rat sacrificed 180 minutes post boron dosing. The cell has a roughly circular shape with diameter ~ 13 μm. The cell nucleus is visible towards the center of the scanned region. The average areal density in the scanned region was 590 +/- 30 $\mu g/cm^2$. The 700 keV proton irradiation produced an alpha particle yield of 4352 counts. The ^{11}B yield map (Figure 6C) and the ^{11}B concentration (mg/kg) map (Figure 6D) appear to show elevated ^{11}B content in the region corresponding to the cell nucleus compared to other cellular regions. The average ^{11}B content in the region corresponding to the cell nucleus is 37 +/- 8 mg/kg, while other cellular regions have an average ^{11}B content of 26 +/- 5 mg/kg. The average ^{11}B content in the cell is 32 +/- 7 mg/kg. ^{11}B concentrations maps from all tumor cells analyzed from animals sacrificed 180 minutes post dosing showed elevated ^{11}B contents in regions corresponding to the location of the cell nucleus compared to other cellular regions.

^{11}B concentrations obtained from $^{11}B(p, \alpha)\ ^{8}Be^*$ analysis and ICPMS ^{11}B analyses.

Table 1 shows average ^{11}B contents in individual tumor cells determined via $^{11}B(p, \alpha)\ ^{8}Be^*$ analysis and average ^{11}B contents in tumors determined via ICP-MS. Students t-tests revealed the ^{11}B contents of individual cells and tumors obtained from animals sacrificed 180 minutes after dosing were significantly lower than those obtained from animals sacrificed 30 minutes after dosing. For each treatment group students t-tests revealed ^{11}B contents of individual cells did not differ significantly from ^{11}B contents of tumors.

Discussion

The results indicate that the $^{11}B(p, \alpha)\ ^{8}Be^{*}$ reaction can be used to image the part per million by weight microdistribution of ^{11}B in biological samples. Analyses can be performed with spatial resolution approaching one micron and minimum detection limits of ~ 1 mg/kg dry weight. Analysis times to acquire sufficient counting statistics to produce meaningful images of ^{11}B microdistribution at concentrations of a few tens of mg/kg in biomedical tissues are ~ 6 hours with a 0.5 nA, 1.5 μm beam spot. Analysis times could be reduced by using higher beam currents, however this can only be achieved by sacrificing spatial resolution as, to first order, the spatial resolution varies directly with square of the beam current.

Analysis times could also be reduced by using particle detectors that subtend a larger solid angle than the 1.6 Sr. used in these measurements. The maximum solid angle attainable is 12.6 Sr. if detectors completely surround the sample. In practice, a solid angle of > 6 Sr. is difficult to achieve as the samples must sit in a translatable target ladder and solid angles greater than 2 Sr. generally require custom designed particle detectors, an expensive option. Even if the solid angle for particle detection were to double over that reported here analysis times would still be ~ 3 hours.

Figures 4, 5 and 6 consistently reveal less clarity in the ^{11}B yield maps than the corresponding STIM maps. There are two major reasons for this. The spatial resolution of the incident proton beam used for the STIM measurements was ~ 0.5 μm while the spatial resolution of the incident proton beam used for the ^{11}B determination was in the range of 1.5 to 2.5 μm. Secondly, the ^{11}B yield maps are hampered by poorer measurement statistics. Of the ^{11}B yield images shown in Figures 4, 5 and 6 the image in Figure 5C was formed from the most number of alpha particles, yet the average number of alpha particles per pixel in this image was ~9. The relative paucity of events in each pixel results in significant statistical variation in the resultant image, which contributes to relatively poor image clarity. In contrast each pixel in a STIM image was formed from the median value of 99 ion energy losses. The median effectively eliminates noise and the image is primarily limited by the statistics of energy straggling and not the statistics of counting individual events.

The thickness of the tissue sections is roughly equivalent to the average tumor cell diameter. As both the $^{11}B(p, \alpha)\ ^{8}Be^*$ and STIM data yield two dimensional projections of a depth averaged distribution the images in Figures 4, 5 and 6 are averages over the whole tissue section depth. This makes identification and interpretation of features within the images more difficult than for the projection of a thinner sample. However, use of thinner samples would require longer irradiation times to produce images with the same counting statistics. Since the irradiation time required to acquire the ^{11}B data is already several hours, use of substantially thinner samples would make analysis times less tractable.

The data in Table 1 suggest 30 % variability in ^{11}B contents of individual cells in tumors from rats treated with f-BPA. Such data are not inconsistent with variations observed in individual cells from compounds used in other therapeutic cancer treatments [30]. There are no significant differences between the $^{11}B(p, \alpha)\ ^{8}Be^*$ derived ^{11}B contents of individual cells and ^{11}B contents of tumors derived using ICP-MS. Minor differences could arise between the two methods as the nuclear microprobe analyses are only sampling individual cells within the tumors whereas the ICP-MS analyses are averages over all tumor components. Both techniques indicate elevated ^{11}B levels in tumors from animals dosed with f-BPA. Furthermore, both techniques suggest ^{11}B levels are higher in tumors from animals sacrificed 30 minutes after dosing than in tumors from animals sacrificed 180 minutes after dosing.

Although not the primary focus of this study, the ^{11}B distribution maps reveal interesting trends in sub-cellular localization. The image in Figure 5 and data in Table 1 indicate that, for animals sacrificed 30 minutes post dosing, ^{11}B appears to be uniformly distributed in tumor cells in a nearly homogeneous pattern. The data in Table 1 also suggest that, although there is less boron in tumor cells at the 180 minute time point than at the 30 minute time point, a greater fraction of cellular boron appears to be concentrated within the cell nucleus at the latter time point. Chandra et al [22] have also observed non-uniform sub-cellular boron distributions in cultured T98G human glioblastoma cells administered f-BPA. The *in-vitro* study by Chandra et al. [22] was on a different cell line, which could partially explain the different pattern of sub-cellular boron distributions observed in the two studies.

Comparison with other boron imaging techniques.

Other analytical procedures have been examined for their suitability in mapping the microdistribution of boron in biomedical tissues. These procedures have included α-track autoradiography [20], electron energy loss spectroscopy (EELS) [21] and secondary ion mass spectroscopy (SIMS) [22].

α-track autoradiography can have sub ppb sensitivity. Furthermore, with thin-section autoradiography, the spatial distribution of sources relative to cells can be obtained from a single section with spatial resolution approaching one micron in ideal cases [35]. By collecting and analyzing serial sections, the 3D microscopic distribution of radionuclide relative to the cellular histology, and therefore the dose rate distribution, can be established [35]. α-track autoradiography has previously been used to determine ^{10}B levels in rats dosed with borotrimethylglycylphenylalanine (BGPA) [21]. In rats bearing intracranial C6 gliosarcomas, α-track autoradiography was able to observe higher ^{10}B levels in tumors than blood or brain. However, in practice sample preparation and data acquisition can be tedious and the spatial resolution of the technique is frequently limited to the range of the alpha particle track [35]. For detection of boron the alpha particle track length ranges from 4 to 14 μm. Such a track length can make NCA subcellular localization studies difficult.

EELS can produce quantitative boron concentrations in tissue sections [21] with spatial resolutions approaching the 50 nm scale. However, the technique typically has a sensitivity of ~ 1000 mg/kg for boron in biological tissues. Because boron levels arising from uptake of NCAs in rodent tumor models and cell lines ranges are typically less than 1000 mg/kg, it is questionable whether EELS has sufficient sensitivity to find widespread use in mapping the microdistribution of boronated NCAs in biological tissues.

SIMS has been utilized in several studies to investigate the distribution of boronated NCAs in biological tissues [22, 36, 37, 38, 39, 40]. The technique can offer sub-micrometer spatial resolution, sensitivities approaching 0.1 mg/kg for bulk analysis of boron in biomedical tissues and analysis times to produce images of boron distribution in NCA dosed cell lines and tumors on the order of several minutes

to an hour. It can also detect and image both ^{10}B and ^{11}B. All these parameters currently surpass those that can be obtained with the $^{11}B(p, \alpha)\ ^{8}Be^*$ nuclear reaction which currently has a spatial resolution approaching one micron, a sensitivity of ~ 1 mg/kg and analysis times of up to six hours. Conversely, the major advantages of the $^{11}B(p, \alpha)\ ^{8}Be^*$ nuclear reaction, are its absolute analytical quantitation and that, compared to SIMS, the analysis causes minimal sample alteration. Quantitative data is generally more difficult to achieve with SIMS and can be prone to greater inaccuracies than with the nuclear microprobe analysis [30]. Secondly, with SIMS the sample surface is sputtered away during analysis. In some instances this can make fine spatial resolution analyses of low levels (< 10 mg/kg) of an isotope in a biological sample difficult to achieve. Conversely, with the nuclear microprobe technique sample loss during irradiation is minimal [30] and detection of low levels of ^{11}B down to the minimum detection limits simply requires a longer irradiation time.

The $^{11}B(p, \alpha)\ ^{8}Be^*$ nuclear reaction offers advantages over alpha track autoradiography and EELS for quantitatively imaging ^{11}B in biological tissues that have been administered boronated NCA analogs. However, the spatial resolution, multi-isotope capability and analysis times that can be achieved with SIMS offer advantages over those that can be achieved with nuclear microprobe analysis. Given multiple trade-offs between quantitation and imaging, sensitivity and general ease of use, SIMS may be the most viable technique to image the microdistribution of boron associated with NCAs in biological tissues. However, when accuracy in quantitation is key to a study the $^{11}B(p, \alpha)\ ^{8}Be^*$ nuclear reaction is well suited for assessing the quantitative microdistribution of ^{11}B in biological tissues.

References.

1. Grossman SA and LK Norris. Adjuvant and neoadjuvant treatment for primary brain tumors in adults. *Seminars in Oncology* 1995; 22: 530-539.
2. Schoenberg BS. Epidemiology of primary intracranial neoplasms: disease distribution and risk factors. In: Salcman M, editor. Neurobiology of Brain Tumors Volume 4. Concepts in Neurosurgery. Baltimore: Williams and Wilkins; 1991. p. 13-18
3. Mueller BA and JG Gurney. Epidemiology of pediatric brain tumors. In: Berger MS, editor. *Pediatric Oncology, Neurosurgical Clinics of North America* 1992; 3(4): 715-721.
4. Pollack IF. Brain Tumors in Children. *New Eng. J. Med.* 1994; 331: 1500-1507.
5. Salford LG, Brun A and S Nirfalk. Ten year survival among patients with supratentorial astrocytoma grade III and IV. *J. Neurosurg* 1988; 69: 506-509.
6. Curran Jr WJ, Scott CB, Horton J, *et al.* Recursive partitioning analysis of prognostic factors in three radiation therapy oncology group malignant glioma trials. *J. Natl. Can. Instit.* 1993; 85: 704-710.
7. Hochberg FH and A Pruitt. Assumptions in the radiotherapy of glioblastoma. *Neurol.* 1980; 30: 907-911.
8. Barth RF, Soloway AH and RG Fairchild. Perspectives in cancer research boron neutron capture therapy of cancer. *Cancer Res.*1990; 50: 1061-1070.
9. Barth RF, Soloway AH, Fairchild RG, *et al.* Boron neutron capture therapy for cancer: realities and prospects. *Cancer* 1992; 70(12): 2995-3007.
10. Sauerwein W. Principles and history of neutron capture therapy. *Strahlenther Onkol.* 1993; 166: 1-6.
11. Haritz D, Gabel D and R Huiskamp. Clinical phase-1 study of $Na_2B_{12}H_{11}SH$ (BSH) in patients with malignant glioma as precondition for boron neutron capture therapy (BNCT). *Int. J. Rad. Onc. Biol. Phys.* 1994; 28(5): 1175-1181.

12. Perks CA, Mill AJ, Constantine BA, *et al.* A review of boron neutron capture therapy (BNCT) and the design and dosimetry of a high-intensity, 24 keV neutron beam for BNCT research. *Brit. J. Rad.* 1988; 61: 1115-1126.

13. Dorn RV. Boron neutron capture therapy (BNCT): a radiation oncology perspective. *Int. J. Rad. Onc. Biol. Phys.* 1994; 28(50): 1189-1201.

14. Barth RF, Matalka KZ, Bailey MQ, *et al.* A nude rat model for neutron capture therapy of human intracerebral melanoma. *Int. J. Radiat. Oncol. Biol. Phys.* 1994; 28: 1079-1088.

15. Coderre JA, Button TM, Micca PL, *et al.* Neutron capture therapy of the 9L rat gliosarcoma using the P-boronphenylalanine-fructose complex. *Int. J. Rad. Oncol. Biol. Phys.* 1994; 30: 643-652.

16. Coderre JA, Rubin P, Freedman A, *et al.* Selective ablation of rat brain tumors by boron neutron capture therapy. *Int. J. Radiat. Oncol. Biol. Phys.* 1994; 28: 1067-1077.

17. Matalka KZ, Barth RF, Staubus AK, *et al.* Boron neutron capture therapy of F98 glioma bearing rats using boronophenylalanine as a capture agent. *Radiat. Res.* 1994; 137: 44-51.

18. Nguyen T, Brownell GL, Holden SA, *et al.* Subcellular distribution of various boron compounds and implications for their efficacy in boron neutron capture therapy by monte carlo simulations. *Radiat. Res.* 1993; 133: 33-40.

19. Codeer JA, Joel DD, Micca PL, *et al.* Control of intracerebral gliosarcomas in rats by boron neutron capture therapy with p-boronophenylalanine. *Radiat. Res.* 1992; 129: 290-296.

20. Takagaki M, Powell W, Sood A, *et al.* Boronated dipeptide borotrimethylglycylphenylalanine as a potential boron carrier in boron neutron capture therapy for malignant brain tumors. *Radiat. Res.* 2001; 156 (1): 118-122.

21. Autry SA, Gandour-Edwards, R Boggan, J *et al.* Subcellular Localization of neutron capture elements using electron energy loss spectroscopic imaging. In: Larsson, B. Crawford, J and R Weinreich, editors. Advances in Neutron Capture Therapy Vol.ii, Chemistry and Biology. Elsevier: Amsterdam; 1997. p. 347-353.

22. Chandra S, Lorey II DR, and DR Smith. Quantitative subcellular SIMS imaging of boron-10 and boron-11 isotopes in the same cell delivered by two combined BNCT drugs: *in vitro* studies on Human Glioblastoma T98G cells. *Radiat. Res.* 2002; 157: 700-710.

23. Sjoland KA, Kristiansson P, and P Tallone. Nuclear reaction analysis of boron for Microbeam analysis of medical samples. *Nucl. Instr. and Meth. In Phys. Res.* 1995; B104: 255-260.

24. Moreton, JA. and HT Delves. Measurement of total boron and ^{10}B concentration and the detection and measurement of elevated ^{10}B levels in biological samples by inductively coupled plasma mass spectrometry using the determination of ^{10}B:^{11}B ratios. *J. Anal. Atom. Spec.* 1999; 14 (10): 1545-1556.

25. Moncoffre N. Analysis of Boron by Charged Particle Bombardment. *Nucl. Instr. and Meth. In Phys. Res.* 1992; B66: 126-138.

26. Lappalainen R, Raisanen J, and A Anttila. Analysis of boron using the (p,α) reaction. *Nucl. Instr. and Meth. In Phys. Res.* 1985; B9: 55-59.

27 Roberts ML, Grant PG, Bench G, *et al.* The Stand-Alone Microprobe at Livermore. *Nucl. Instr. and Meth. In Phys. Res.* 1999; B158: 24-30.

28 Antolak AJ, Bench G and DH Morse. IMAP: A Complete Ion Micro-Analysis Package for the Nuclear Microprobe. *Nucl. Instr. and Meth. In Phys. Res.*, 1994; B85: 597-601.

29. Autry-Conwell SA, Hou Y, Edwards B, *et al.* Inductively coupled plasma mass spectrometry for quantitative biodistribution analysis of neutron capture agents in tissue. *Trans. Am. Nucl. Soc.* 1998; 80: 77-78.

30. Mauthe RJ, Sideras-Haddad E, Turteltaub KW, *et al.* Quantitative Imaging Microscopy for the Sensitive Detection of Administered Metal Containing Drugs in single cells and tissue slices-A demonstration using Platinum based chemotherapeutic Agents. *J. Pharm. Biomed. Anal.* 1998; 17: 651-663.

31. Barth RF, Soloway AH, Goodman JH, *et al.* Boron neutron capture therapy in brain tumors: An emerging therapeutic modality. *Neurosurgery* 1999; 44: 433-451.

32. Lefevre HW, Schofield RMS, Overley JC, *et al.* Scanning Transmission Ion Microscopy as it complements Particle Induced X-ray Emission microscopy. *Scan. Micr.* 1987; 1: 879-889.

33. Bench, G. Scanning Transmission Ion microscopy. *Ph. D. Thesis.* University of Melbourne, Melbourne, Australia; 1991.

34. Lefevre HW, Schofield RMS, Bench G, *et al.* STIM with Energy Loss Contrast: An Imaging Modality Unique to MeV Ions. *Nucl. Instr. and Meth. In Phys. Res* . 1991; B54: 363-370.

35. Humm JL, Macklis R.M, Lu,XQ, *et al.* The spatial accuracy of cellular dose estimates obtained from 3D reconstructed serial tissue autoradiographs. *Phys. Med. Biol.* 1995; 40 (1): 163-180

36. Zha X, Ausserer WA and GH Morrison. Quantitative imaging of a radiotherapeutic drug $Na_2B_{12}H_{11}SH$ at subcellular resolution in tissue cultures using ion microscopy. *Cancer Res.* 1992; 52: 5219-5222.

37. Chandra S, Lorey II DR, Lessig SL, *et al.* Quantitative imaging of boron from BPA and BSH in glioblastoma cells with ion microscopy. In: Larsson B, Crawford J and R. Weinreich, editors. Advances in Neutron Capture Therapy Vol.ii, Chemistry and Biology. Elsevier: Amsterdam; 1997. p 315-320.

38. Smith DR, Chandra S, Coderre JA *et al.* Ion microscopy imaging of ^{10}B from pboronophenylalanine in a brain tumor model for boron neutron capture therapy. *Cancer Res.* 1996; 56: 4302-4306.

39. Morris GM, Smith DR, Patel H, *et al.* Boron microlocalization in oral mucosal tissue: Implications for boron neutron capture therapy. *Br. J. Cancer* 2000; 82: 1764-1771.

40. Smith DR, Chandra S, Coderre JA, *et al.* Ion microscopy imaging of boron from pboronophenylalanine in surgically acquired samples of human brain tumor tissue. In: Hawthorne ME, Shelly K and RJ Wiersema , editors. Frontiers in Neutron Capture Therapy. New York : Kluwer Academic; 2001. p. 899-904.

Tables.

Table 1: ^{11}B contents in tumors and individual tumor cells. The first column shows the animal treatment. "Dosed 30 minutes" corresponds to animals that were dosed with f-BPA and sacrificed 30 minutes post dosing, while "Dosed 180 minutes" corresponds to animals that were dosed with f-BPA and sacrificed 180 minutes post dosing. The second column shows the number of cells analyzed with the $^{11}B(p, \alpha)$ $^{8}Be^*$ nuclear reaction. The third column shows average ^{11}B content in the cells expressed as a mean +/- standard deviation of the individual cell measurements. In this column, MDL stands for minimum detection limit. The fourth column shows the average ratio of ^{11}B content in the cell nucleus to other cellular regions for each group of cells analyzed. The final column shows average ^{11}B concentrations in the tumors determined via ICPMS.

Animal Group	**Cells analyzed**	**^{11}B per cell (mg/kg)**	**Ratio of ^{11}B content in cell nucleus to other cellular regions**	**^{11}B per tumor (mg/kg)**
Control	6	< MDL	Not applicable	0.3 +/- 0.1
Dosed 30 minutes	12	55 +/- 19	1.0 +/- 0.2	48 +/- 4[2]
Dosed 180 minutes	12	29 +/- 9[1]	1.4 +/- 0.3	33 +/- 2[1,2]

[1] $P < 0.05$ when compared to "Dosed 30 minute" samples using students t-test.

[2] $P > 0.05$ when compared to individual cell analyses using students t-test.

Figure Captions.

Figure 1: Schematic diagram of the experimental arrangement used to perform the $^{11}B(p, \alpha)\ ^{8}Be^*$ analysis. For STIM analysis a particle detector is inserted between the sample and Faraday cup and is used to measure the residual energies of ions after passing through the sample.

Figure 2: Energy spectra of scattered particles obtained with a 700 keV incident proton beam. Figure 2a is the energy spectrum obtained from a freeze dried liver tissue sample. Figure 2b is the energy spectrum obtained from an 1800 angstrom thick B_5N film. The dashed vertical lines at channels 460 and 870 in each spectrum indicate the location of the energy window used to determine alpha particle yields from the $^{11}B(p, \alpha)\ ^{8}Be^*$ reaction.

Figure 3: Curve of α yield versus incident proton energy for the $^{11}B(p, \alpha)\ ^{8}Be^*$. The yield is calculated for the energy window shown in Figure 3 between channels 460 and 870. The solid line connecting the data points is a cubic spline and is shown to guide the eye.

Figure 4: 28.3 x 15.1 μm^2 images resulting from the analysis of a cell in a tumor from a rat not dosed with boron. Figure 4A is an image of tissue areal density consisting of 118 x 58 pixels. The number of pixels in this image were subsequently reduced to 59 x 29 pixels by averaging the areal densities of each group 2 x 2 pixels to produce the Figure 4B. The pixel reduction was performed so that corresponding areal density and boron images would have the same image size and same pixel dimensions. Figure 4C is image of the corresponding ^{11}B yield (ng/cm^2) and was obtained with a ~1 nA, 2.5 μm diameter beam. The irradiation time was 5.5 hours and a dose of 20 μC was deposited to the scan area. Figure 4D is an image of the ^{11}B concentration (mg/kg). This final image was obtained by dividing the ^{11}B yield image (4C) pixel by pixel by the registered areal density image (4B).

Figure 5: 28.3 x 15.1 μm^2 images resulting from the analysis of a tumor cell from a rat dosed with boron and sacrificed 30 minutes post dosing. Figure 5A is an image of tissue areal density consisting of 118 x 58 pixels. The number of pixels in this image were subsequently reduced to 59 x 29 by averaging to produce the image in Figure 5B. Figure 5C is an image of the corresponding ^{11}B yield (ng/cm^2) and was obtained with an ~ 1 nA, 2.5 μm diameter beam. The irradiation time was 6 hours and a dose of 20 μC was deposited to the scan area. Figure 5D is the corresponding image of the ^{11}B concentration (mg/kg).

Figure 6: 18.7 x 15.1 μm^2 images resulting from the analysis of a tumor cell from a rat dosed with boron and sacrificed 180 minutes post dosing. Figure 6A is an image of tissue areal density consisting of 72 x 58 pixels. The number of pixels in this image were subsequently reduced to 36 x 29 by averaging to produce the image in Figure 6B. Figure 6C is an image of the corresponding ^{11}B yield (ng/cm^2) and was obtained with a ~ 0.5 nA, 1.5 μm diameter beam. The irradiation time was 6 hours and a dose of 10 μC was deposited to the scan area. Figure 6D is the corresponding image of the ^{11}B concentration (mg/kg).

Figures.

Figure 1:

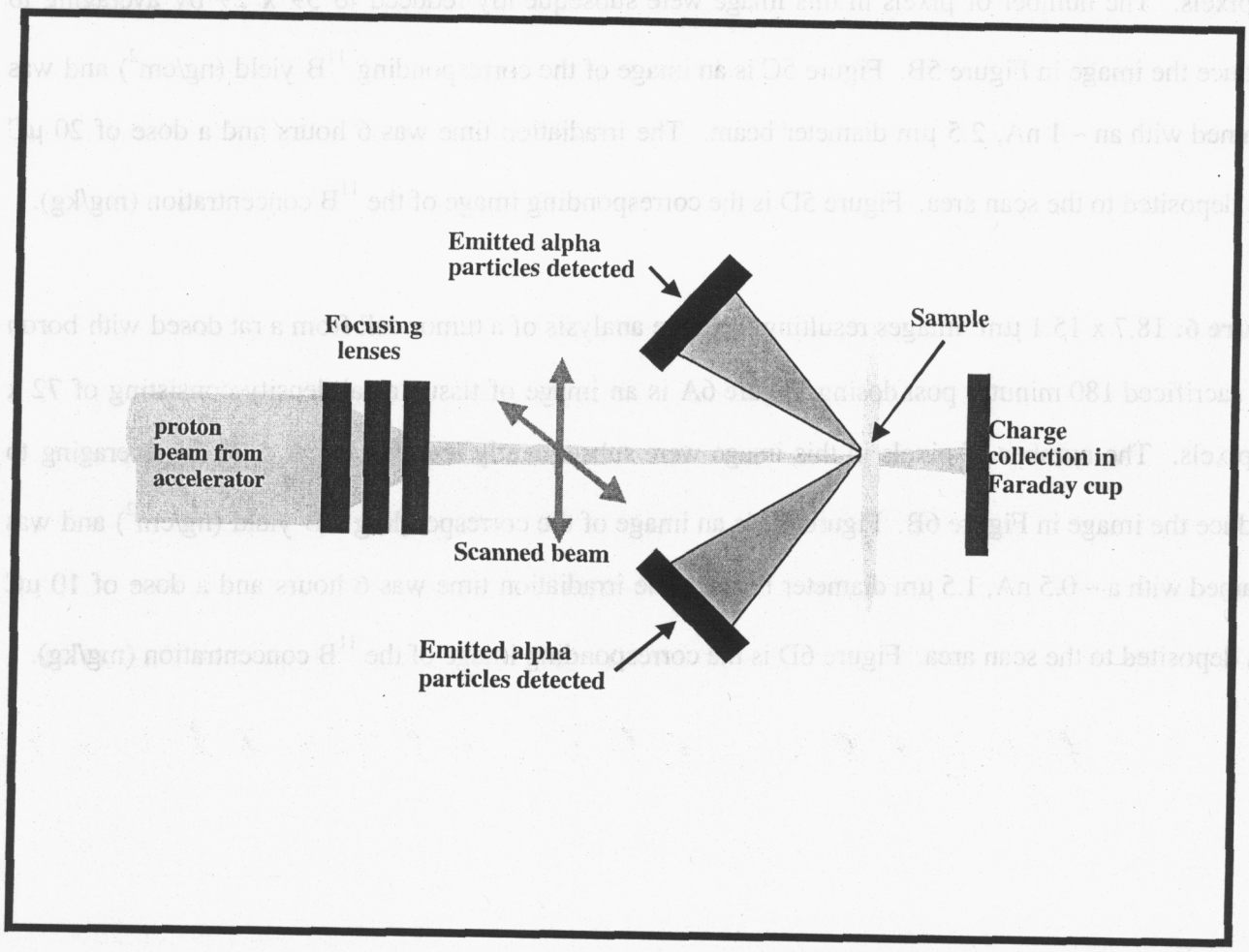

Figure 3:

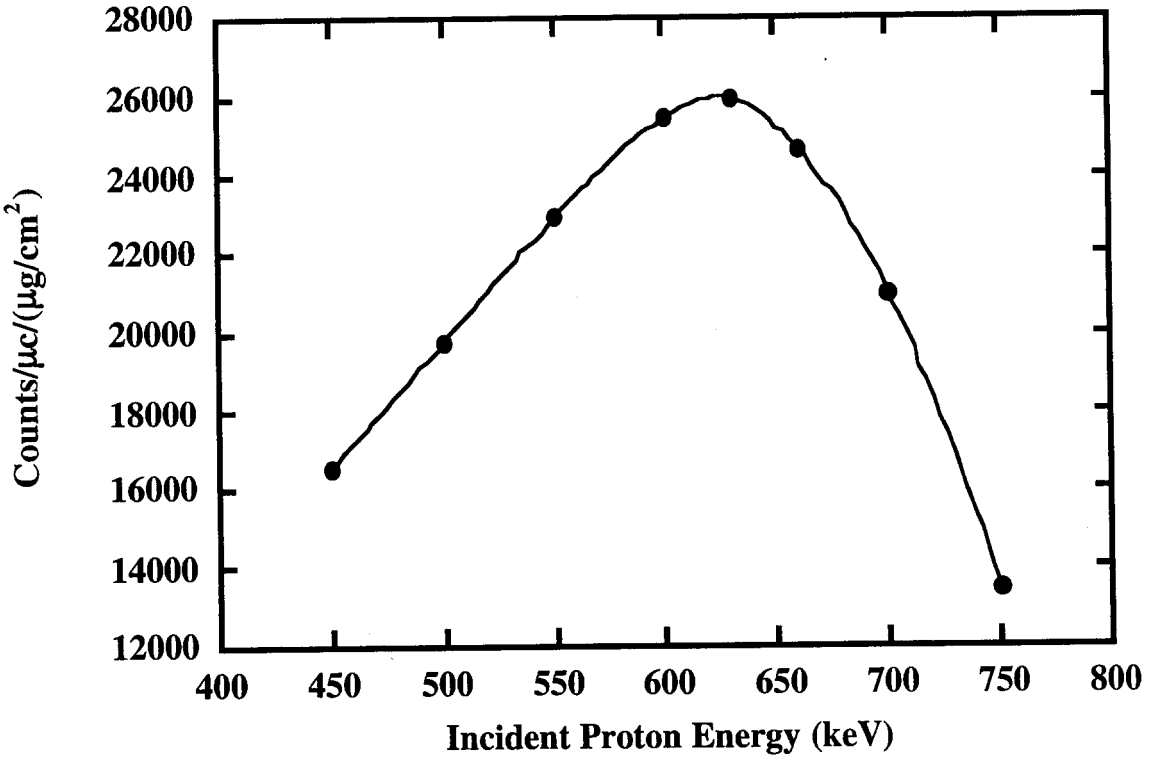
28000
26000
24000
22000
20000
18000
16000
14000
12000
Counts/μc/(μg/cm²)
400
450
500
550
600
650
700
750
800
Incident Proton Energy (keV)

Figure 2:

A

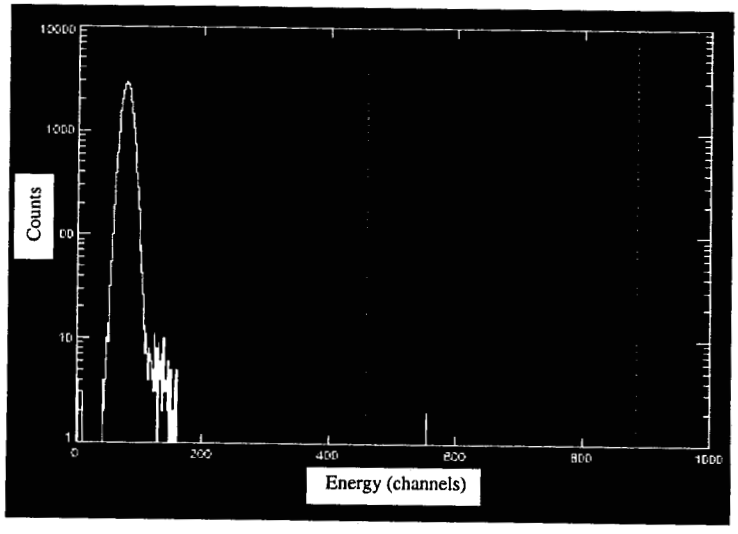
10000
1000
Counts
10
1
0
200
400
800
1000
Energy (channels)

B

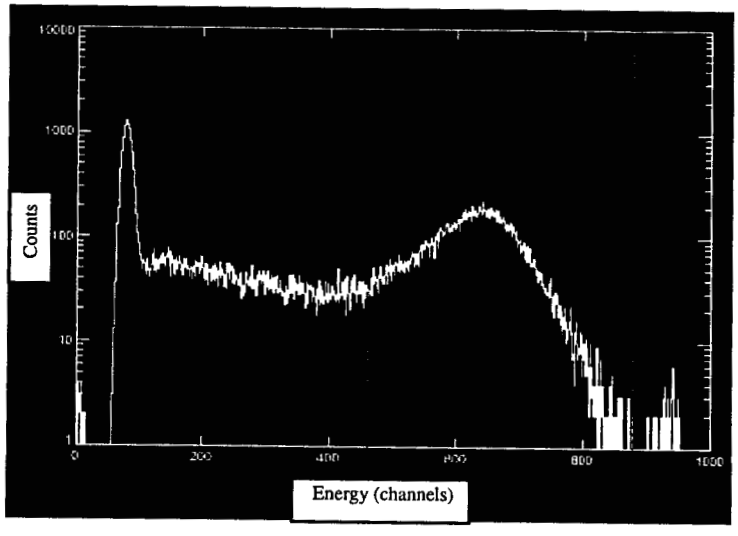
10000
1000
Counts
100
10
1
0
200
400
800
1000
Energy (channels)

Figure 4:

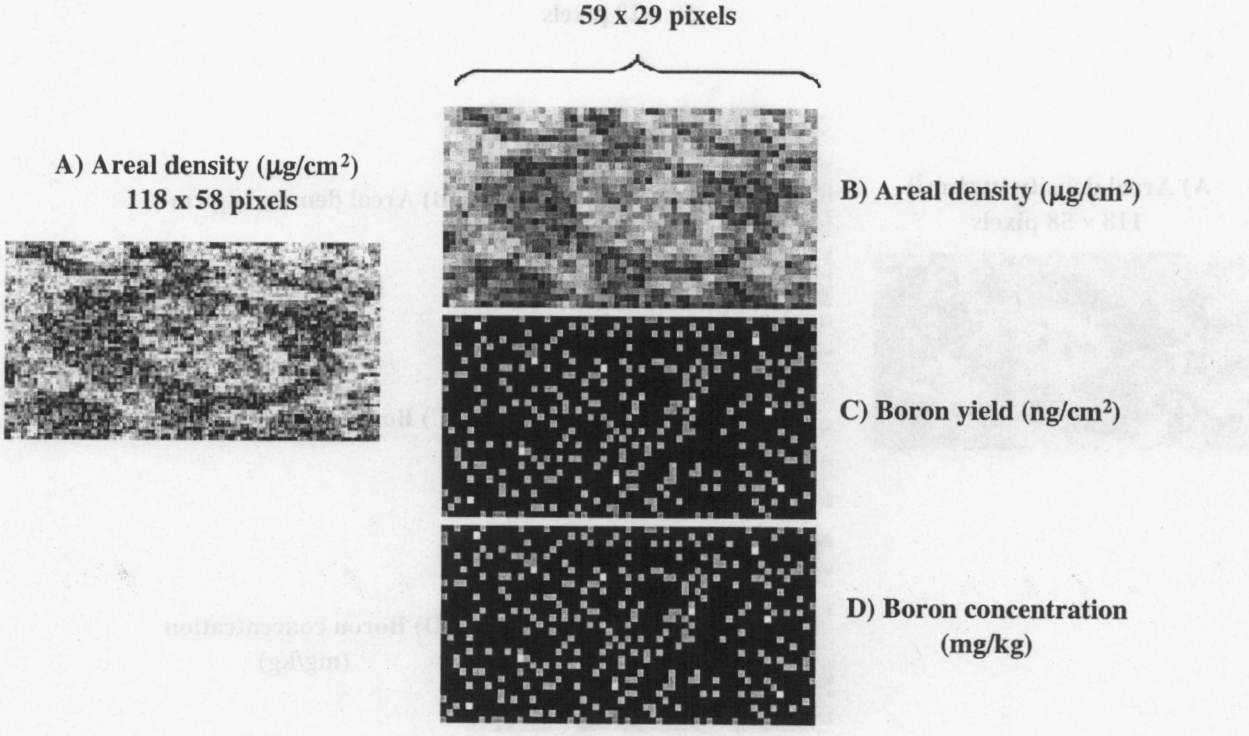
59 x 29 pixels
A) Areal density (μg/cm²)
118 x 58 pixels
B) Areal density (μg/cm²)
C) Boron yield (ng/cm²)
D) Boron concentration
(mg/kg)

Figure 5:

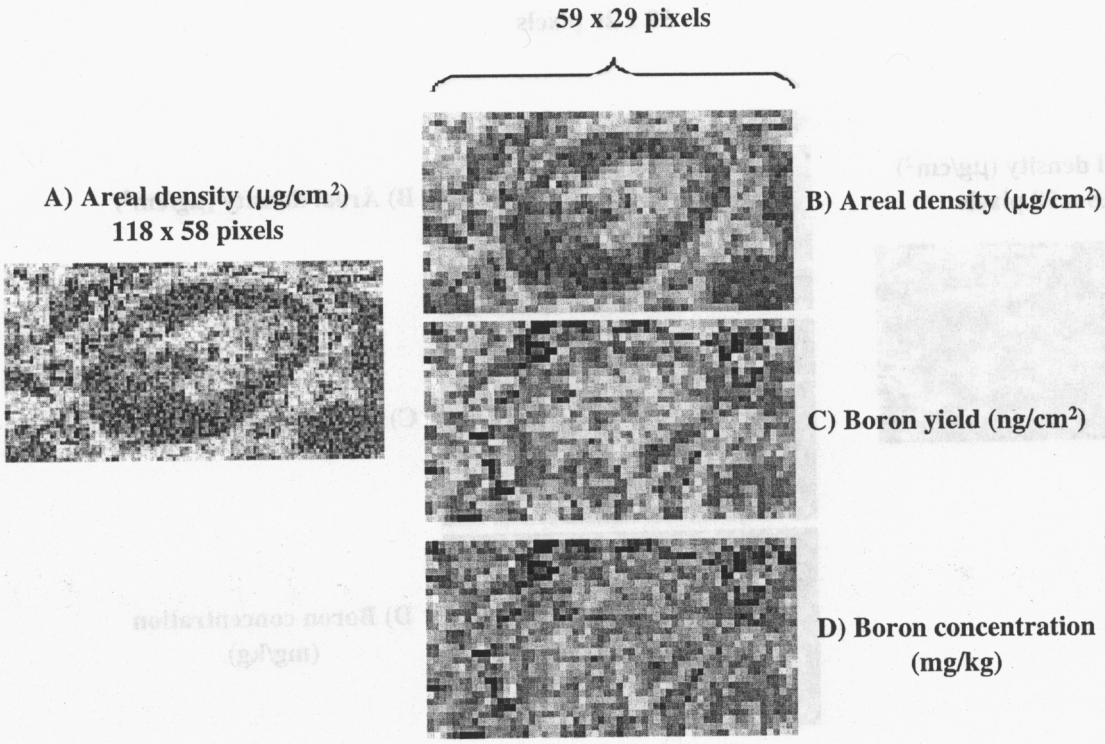
59 x 29 pixels
A) Areal density (μg/cm²)
118 x 58 pixels
B) Areal density (μg/cm²)
C) Boron yield (ng/cm²)
D) Boron concentration
(mg/kg)

Figure 6:

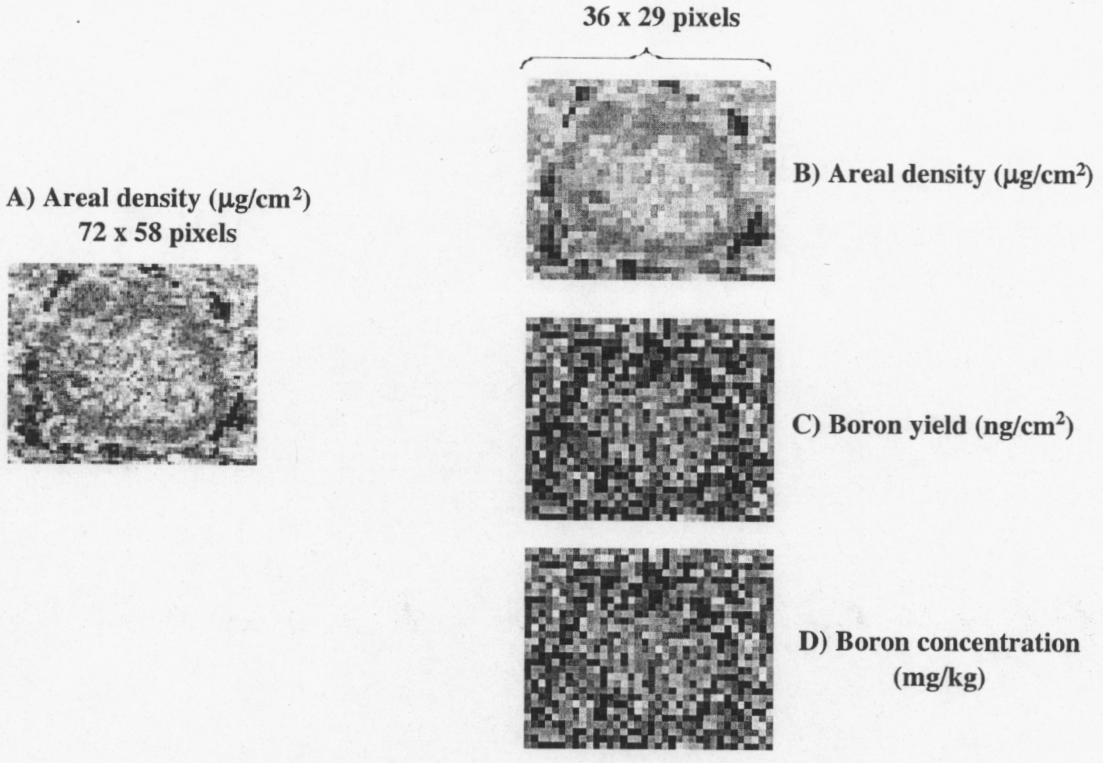
36 x 29 pixels
A) Areal density (μg/cm²)
72 x 58 pixels
B) Areal density (μg/cm²)
C) Boron yield (ng/cm²)
D) Boron concentration
(mg/kg)